processes

MDPI

Article

Fault Diagnosis of Rolling Bearings Based on Adaptive Denoising Residual Network

Yiwen Chen [1], Xinggui Zeng [2,3,*] and Haisheng Huang [3,*]

[1] School of Mechanical-Electrical and Information Engineering, Putian University, Putian 351100, China; enyiwen@163.com
[2] Engineering Research Center of Disaster Prevention and Mitigation of Southeast Coastal Engineering Structures, Fujian Province University, Putian 351100, China
[3] School of Civil Engineering, Putian University, Putian 351100, China
* Correspondence: yllzxg2012@163.com (X.Z.); deepseawdd@163.com (H.H.)

Abstract: To address the vulnerability of rolling bearings to noise interference in industrial settings, along with the problems of weak noise resilience and inadequate generalization in conventional residual network frameworks, this study introduces an adaptive denoising residual network (AD-ResNet) for diagnosing rolling bearing faults. Initially, the sensors collect the bearing vibration signals, which are then converted into two-dimensional grayscale images through the application of a continuous wavelet transform. Then, a spatial adaptive denoising network (SADNet) architecture is incorporated to comprehensively extract multi-scale information from noisy images. By exploiting the improved pyramid squeeze attention (IPSA) module, which excels in extracting representative features from channel attention vectors, this unit substitutes the standard convolutional layers present in typical residual networks. Ultimately, this model was validated through experiments using publicly available bearing datasets from CWRU and HUST. The findings suggest that with −6 dB Gaussian white noise, the average accuracy of recognition achieves a rate of 90.96%. In scenarios of fluctuating speeds accompanied by strong noise, the recognition accuracy can reach 89.54%, while the training time per cycle averages merely 3.65 s. When compared to other widely utilized fault diagnosis techniques, the approach described in this paper exhibits enhanced noise resistance and better generalization capabilities.

Keywords: fault diagnosis; rolling bearing; continuous wavelet transform; residual neural network

check for updates

Academic Editor: Wei Sun

Received: 7 December 2024
Revised: 31 December 2024
Accepted: 7 January 2025
Published: 8 January 2025

Citation: Chen, Y.; Zeng, X.; Huang, H. Fault Diagnosis of Rolling Bearings Based on Adaptive Denoising Residual Network. *Processes* **2025**, *13*, 151. https://doi.org/10.3390/pr13010151

Copyright: © 2025 by the authors. Licensee MDPI, Basel, Switzerland. This article is an open access article distributed under the terms and conditions of the Creative Commons Attribution (CC BY) license (https://creativecommons.org/licenses/by/4.0/).

1. Introduction

Rolling bearings, which serve as essential components in rotary mechanical transmission devices, are often referred to as the "joints of industry". The proper functioning of other components is directly influenced by the condition of these bearings [1]. In southeastern coastal areas, environmental factors like elevated temperatures and salt mist can cause rolling bearings to fail after extended operation. Such failures may rapidly lead to a chain reaction, damaging other components and resulting in direct or indirect economic losses [2,3]. Therefore, it is crucial to monitor rolling bearings in real time and detect early failures promptly.

With the ongoing advancement of fault diagnosis technology, intelligent fault diagnosis methods are steadily becoming the mainstream in this field [4]. During the signal processing phase, time-frequency analysis methods, such as short-time Fourier transform,

empirical mode decomposition, and wavelet transform, are commonly used to extract relevant feature information from one-dimensional vibration signals. Subsequently, machine learning approaches, such as multilayer perceptron [5], random forest [6], and support vector machine [7], are utilized for fault classification. Rai et al. [8] implemented a technique that integrates empirical mode decomposition with k-medoids clustering to diagnose rolling bearings. Zhu et al. [9] utilized principal component analysis to extract main eigenvalues and eigenvectors from fault features, followed by using a deep belief network to conduct fault classification on the modified samples. Although these machine learning techniques, being traditional intelligent fault diagnosis methods, perform well under specific conditions, they depend significantly on expert knowledge and are limited in identifying deeper fault signal features.

Recently, deep learning-based fault diagnosis methods have seen widespread application. These methods can create a mapping between fault signals and categories, exhibiting strong automatic feature extraction capabilities that address the limitations of traditional approaches [10]. One prominent example is convolutional neural networks, which share weights and extract translation-invariant features [11]. To tackle the challenge of vibration sensors being prone to noise interference in industrial settings, Zhang et al. [12] introduced a wide-kernel convolutional neural network that performs effectively in high-frequency noise environments by using a "wide convolution kernel in the first layer and smaller kernels in subsequent layers" strategy. Wang et al. [13] proposed a convolutional neural network with a squeeze-and-excitation mechanism to help the model focus on principal features, thereby improving fault diagnosis. These approaches, however, predominantly depend on conventional convolutional layers, potentially complicating fault detection under intricate real-world conditions like simultaneous load variations and noise. To tackle this challenge, Xiong et al. [14] utilized time-frequency images derived from short-time Fourier transform as input into deep residual networks for fault classification, achieving effective rolling bearing fault diagnosis. Similarly, Tian et al. [15] incorporated the squeeze-and-excitation network structure into deep residual networks, enabling accurate bearing fault diagnosis even with noise and load changes. To tackle the problem of low diagnostic efficiency in complex environments, Zhang et al. [16] combined a channel-spatial attention mechanism with deep residual networks, demonstrating good fault recognition under varying conditions. Chu et al. [17] crafted a multi-scale convolutional model that employs diverse dilation rates and multi-attention mechanisms, specifically designed based on convolutional kernel characteristics, to extract more detailed features from raw signals and minimize the influence of redundant information within feature maps. In recent times, transformer-based models have seen widespread adoption by numerous scholars in the fault diagnosis domain. Hou et al. [18] melded attention mechanisms with vision transformers to create a multi-feature parallel fusion encoder, facilitating swift extraction of both local and global fault characteristics. Ji et al. [19] advanced the vision transformer by adding a patch feature extraction module, emphasizing the priority extraction of key fault signal features. While deep learning algorithms exhibit high accuracy in fault diagnosis, they continue to grapple with several challenges. For one, traditional algorithms with fixed receptive fields can struggle with vanishing gradients in complex environments, such as when strong noise, load, and speed fluctuations coexist. Additionally, in practical industrial environments, intelligent fault diagnosis primarily depends on edge devices, but prevalent deep learning algorithms—like various transformer model variants—are computationally intensive and reliant on large data sets, often delaying early fault detection. Consequently, ongoing research is aimed at refining algorithms to bolster their effectiveness in intricate scenarios and early fault identification. This line of research holds crucial importance for the advancement of fault diagnosis in the rotating machinery sector.

In response to the outlined challenges, this research introduces an Adaptive Denoising Residual Network model, known as AD-ResNet, which seeks to remedy problems in fault signal feature extraction and generalization shortcomings induced by strong noise, load changes, and variations in speed. The principal contributions of this study are as follows:

(1) RQ1: How can the difficulty of extracting fault features and the confusion in complex conditions with strong noise that commonly used algorithms face to be alleviated? To tackle this, we integrated a spatial adaptive denoising network structure within the residual neural network architecture. For signals with strong noise, this structure employs a multi-scale encoder−decoder architecture to sample and weigh features at various scales. It estimates offsets, removing noise and reconstructing textures progressively from coarse to fine. This denoising approach is vital when processing early fault data laden with noise, as it not only successfully extracts multi-scale information but also preserves high fault detection accuracy.

(2) RQ2: How can the sensitivity of standard convolution layers in residual blocks be overcome to scale changes and their high computational cost? In response, we developed an enhanced pyramid squeeze attention module to replace the existing standard convolution layers. After noise reduction, this enhanced module can gather channel attention vectors, multi-scale spatial information, and key cross-dimensional features within the channel attention vectors. This approach not only minimizes redundant computations but also boosts the learning of representative features. This modification improves the model's capability to extract features under complex conditions and speeds up convergence.

The structure of the rest of this paper is as follows: Section 2 covers the related works. Section 3 elaborates on the theoretical foundations. Section 4 details the design of the proposed model. Section 5 examines its application on both the CWRU and HUST datasets. Lastly, Section 6 summarizes the primary conclusions and proposes directions for future research.

2. Related Works

2.1. CNN-Based Models for Fault Diagnosis

Convolutional neural networks (CNNs) are extensively used in diagnosing faults in rolling bearings due to their robust feature extraction capabilities and parameter sharing [20]. CNNs can learn fault characteristics effectively through multiple convolutional layer stacking and display excellent generalization abilities. Researchers focus on creating noise-resistant structures to address noise issues in industrial settings more efficiently. Che et al. [21] integrated stacked denoising autoencoders (SDAEs) with CNNs to bolster the model's capacity to manage noisy signals. The non-local full convolutional neural network (NL-FCNN) [22] built non-local blocks using Leaky-ReLU activation functions and non-local means, which greatly enhanced denoising capabilities. Findings suggested that under a signal-to-noise ratio (SNR) of −6 dB, this approach achieved an 85.16% recognition accuracy on the CWRU dataset under constant load. Despite the ability of these noise-resistant models to extract fault characteristics from noisy signals effectively, having relatively few CNN parameters may restrict expressive power under complex and dynamic conditions, thereby degrading generalization performance.

2.2. ResNet-Based Models for Fault Diagnosis

Deep residual networks, known as ResNet, are extensively used in fault diagnosis because they effectively address the gradient vanishing problem encountered in training deep networks [23]. The adaptability of the ResNet structure allows for easy adjustment of network depth (like ResNet-18 and ResNet-50) to accommodate varying data sizes, demon-

strating its stable performance and wide applicability in numerous industrial monitoring and diagnostic tasks. To boost ResNet's diagnostic capability, researchers have refined and optimized its convolutional layers and residual constructs. For instance, Lei et al. [24] used depthwise separable and pointwise convolutions to replace standard convolutional layers of ResNet, which cuts down computational complexity and amplifies nonlinear expressive abilities. The outcomes indicate that this approach achieves a 90.19% average accuracy under varying speed settings on the CWRU dataset. In addition, Fu et al. [25] integrated singular value decomposition (SVD) pooling and global SVD pooling (GSP) in the traditional residual networks' pooling and fully connected layers, thus mitigating overfitting risks and enhancing feature extraction. Even though ResNet excels in preserving the completeness of feature information, there is potential for advancement in managing multi-scale features and improving computational efficiency.

2.3. ViT-Based Fault Diagnosis Models

The vision transformer (ViT) is a model built around the self-attention mechanism, which captures significant interest in fault diagnosis due to its strong feature representation and ability to process information in parallel [26]. As research evolves, many variants and enhanced versions of the ViT have surfaced, aiming to boost its adaptability for various tasks and conditions, such as vicinity vision transformer (VVT) [27], dual vision transformer (Dual-ViT) [28], and dendritic learning-incorporated vision transformer (DVT) [29]. However, ViT models tend to have high computational complexity, and their effectiveness with small sample datasets is somewhat constrained. To address these challenges, researchers have focused on refining and optimizing ViTs. For example, Li et al. [30] suggested a lightweight multi-feature fusion ViT that decreases computational demands by employing a local perception module with multi-scale wide convolution. Xu et al. [31] investigated using a multi-information fusion vision transformer model for diagnosing faults in rolling bearings, with the goal of enhancing diagnostic accuracy for small sample vibrational data. Zhang et al. [32] combined dual-stream adaptive deep residual shrinkage blocks (DSA-DRSBs) with a ViT to extract essential fault features from limited samples. Results from experiments on a custom small sample dataset demonstrated an average recognition accuracy of 91.14%. A continuing challenge is to sustain effective feature extraction in ViT while lowering computational costs.

In conclusion, models for fault diagnosis utilizing the CNN, ResNet, and ViT display distinct strengths in the arena of intelligent fault diagnosis. The CNN model has achieved notable advancements in feature extraction and processing structured data automatically. However, its ability to handle complex noise and load changes could be further enhanced. ResNet solves the challenge of vanishing gradients in deep networks by utilizing residual structures, enabling extraction of deeper features. Nonetheless, it demands careful design planning of the model's architecture. The ViT's introduction has paved new paths for fault diagnosis, as its global self-attention mechanism boosts the efficiency of feature extraction. However, its computational demands and reliance on large data volumes restrict the ViT's use in real-time industrial settings. Even though these advances have contributed significantly to fault diagnosis, there is still a need for improved accuracy in early fault identification and efficiency in real-time diagnostics under challenging conditions such as high noise levels and fluctuations in speed and load. To tackle these challenges, this study presents a spatial adaptive denoising framework within residual networks and suggests an augmented pyramid squeeze attention module aimed at boosting robustness and precision in extracting fault features amidst complex conditions. This strategy introduces an innovative approach to diagnosing rolling bearing faults and establishes a groundwork for advancements in intelligent fault diagnosis.

3. Theoretical Foundation

3.1. Continuous Wavelet Transform

The Continuous Wavelet Transform (CWT) serves as a data preprocessing method extensively employed for the extraction of time-domain features and corresponding frequency-domain spectral details [33]. This technique converts the original signal into a time-frequency distribution, building a dual representation of the signal across time and frequency domains, thereby creating a time-frequency image. For any given signal $x(t)$, its CWT is calculated via convolution with a complex conjugate, specifically defined as:

$$W(s,\tau) = \langle x(t), \psi_{s,\tau} \rangle = \frac{1}{\sqrt{s}} \int x(t) \psi^* \left(\frac{t-\tau}{s} \right) dt \quad (1)$$

In this equation, the scale parameter s represents its inverse relationship with frequency; τ is the shift parameter; ψ^* denotes the complex conjugate, and $\psi_{s,\tau}$ identifies the mother wavelet, specifically the Morlet wavelet.

Applying this formula, the signal $x(t)$ is broken down into a sequence of wavelet coefficients. Through these convolution operations, $x(t)$ undergoes transformation and projection in both temporal and spectral dimensions, transforming the original one-dimensional series into a two-dimensional time-frequency visualization. In this paper's experimental section, each class's data within the dataset are subjected to overlap sampling with signals of length 1024, with calculations based on the following formula:

$$N = \frac{L - L_1}{M} + 1 \quad (2)$$

where L is the total length of the one-dimensional signal; L_1 indicates the segment length; M defines the stride, and N is the sample count per class.

Time-frequency images derived from the HUST bearing data using the CWT are depicted in Figure 1.

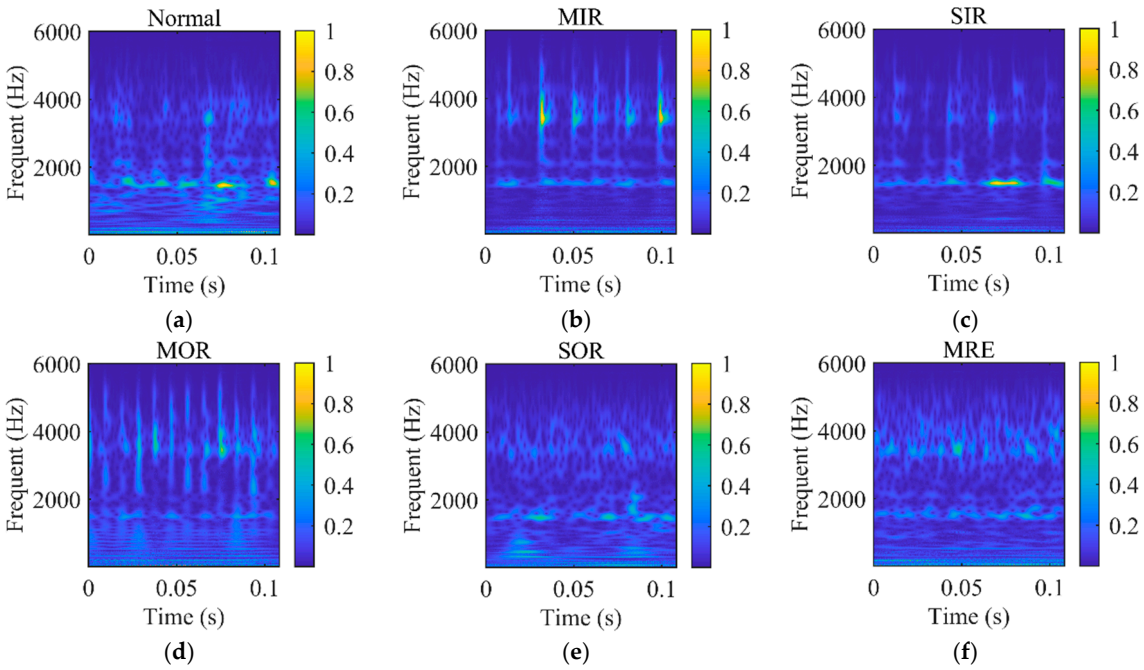


Figure 1. Selected time-frequency representations of various bearing fault conditions: (**a**) normal condition; (**b**) inner ring fault at a moderate level; (**c**) inner ring fault at a severe level; (**d**) outer ring fault at a moderate level; (**e**) outer ring fault at a severe level; (**f**) rolling element fault at a moderate level.

3.2. Deep Residual Networks

Increasing the depth of neural networks raises the training complexity of convolutional neural network models. To tackle this issue, He et al. [34] introduced the deep residual networks (ResNet) model in 2015. This approach significantly decreases the training complexity of deep neural networks by integrating identity mappings into standard convolutional neural networks.

ResNet consists of several residual blocks, each forming a core part of the model. According to Figure 2, a residual block incorporates layers such as convolutional (Conv2d), batch normalization (BN), and ReLU activation functions. Inside a residual block, input data traverse both the residual path and the identity mapping path, and they are combined before passing through the ReLU activation function. Owing to the direct connection between the input and output in the residual block, effective error backpropagation is facilitated, which improves both the model's training efficiency and generalization performance [35]. The operation of the residual block is expressed through the subsequent equation:

$$G(x) = F(x) + x \tag{3}$$

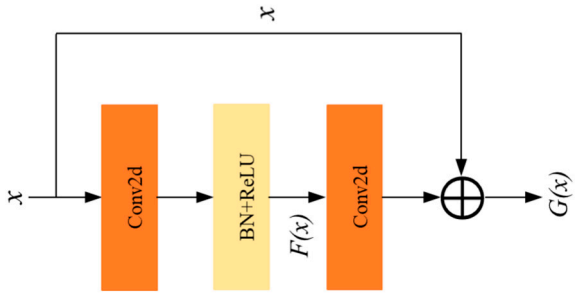


Figure 2. ResNet residual block [34].

In this equation, $G(x)$ signifies the resulting identity mapping function; $F(x)$ signifies the residual mapping; and x denotes the input to the residual block.

3.3. Spatial-Adaptive Denoising Network

The traditional residual network structure employed for extracting features from bearing fault images often contains not only fault-related information but also noise originating from the industrial environment. Conventional convolution operations can accumulate background noise during feature extraction, diminishing the focus on important features and adversely affecting diagnostic accuracy. To enhance the model's emphasis on essential features and mitigate the influence of noise, this paper introduces the spatial-adaptive denoising network (SADNet) [36] framework. This network architecture efficiently extracts relevant features from intricate image content and retrieves details and textures from substantial noise. The central component of the adaptive denoising network is the residual spatial-adaptive block (RSAB), which utilizes deformable convolutions to weight spatially relevant features during sampling [36]. By integrating an encoder−decoder architecture with upsampling and downsampling mechanisms, it progressively collects multi-scale feature information, calculates offsets and eliminates noise progressively from coarse to fine. This process ultimately produces high-quality, denoised images. Figure 3 illustrates the structural diagram of this network.

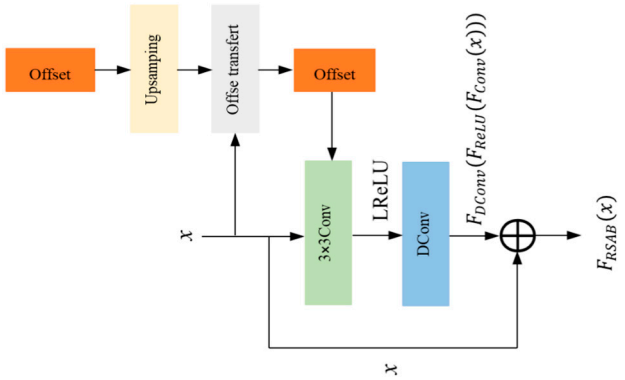


Figure 3. Residual spatial-adaptive block [36].

The RSAB includes a deformable convolution, a standard convolution, and a short skip connection and can be described as:

$$F_{RSAB}(x) = F_{DConv}(F_{ReLU}(F_{Conv}(x))) + x \tag{4}$$

where F_{Conv} is the standard convolution and F_{ReLU} is the Leaky activation function.

The RSAB adjusts the offsets Δp^{s-1} and modulation scalars Δm^{s-1} from the previous scale to the current scale s and utilizes $\{\Delta p^{s-1}, \Delta m^{s-1}\}$ together with the input features x^s to determine $\{\Delta p^s, \Delta m^s\}$ [36], thereby refining the offsets from a coarse approximation to a fine estimation. By employing the small-scale offsets as an initial guide, it becomes possible to identify relevant features more accurately on a larger scale. The offset transformation formula is described as follows:

$$\{\Delta p^s, \Delta m^s\} = F_{offset}\left(x^s, F_{up}\left(\left\{\Delta p^{s-1}, \Delta m^{s-1}\right\}\right)\right) \tag{5}$$

where F_{offset} and F_{up} denote the offset transformation and upsampling functions, respectively.

3.4. Improved Pyramid Split Attention Module

To resolve the problem where channel attention and spatial attention fail to establish long-range dependencies within channels, Hu et al. [37] introduced the pyramid split attention (PSA) module. Inspired by spatial-channel reconstruction convolutions [38], this paper enhances the PSA module to extract multi-scale spatial information from channel-specific feature maps while minimizing redundant information during the extraction process. Figure 4 illustrates the architecture of the improved pyramid split attention (IPSA) module.

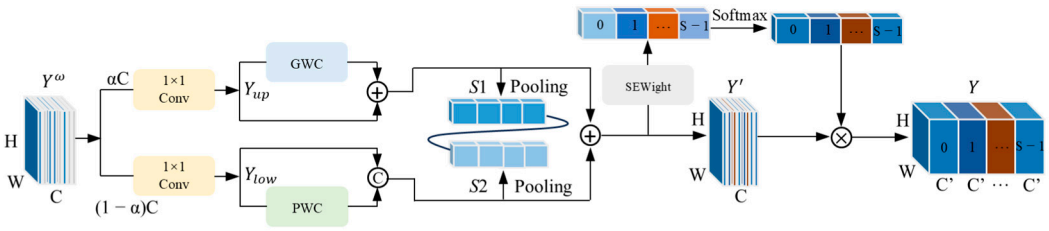


Figure 4. IPSA module.

Initially, the IPSA module separates the input feature map Y^{ω} into two portions: αC and $(1 - \alpha)$C, where the channel split ratio $0 \leq \alpha \leq 1$ is represented. To improve computational efficiency, a 1×1 convolution is employed to decrease the channel count.

After the splitting operation, Y^{ω} is segregated into an upper-layer feature map, denoted as Y_{up}, and the lower-layer feature map, referred to as Y_{low}.

The segments αC and $(1-\alpha)$C are then transformed separately in the upper and lower layers. Efficient convolutions, GWC and PWC, are applied to extract key features and supplementary detailed features, respectively. These features are subsequently combined through channel-wise addition to produce the feature map Y':

$$Y' = \left(M^{G} Y_{up} + M^{P_1} Y_{up}\right) \oplus \left(M^{P_2} Y_{low} \cup Y_{low}\right) \tag{6}$$

Within the formula, M^{G}, M^{P_1}, and M^{P_2} represent the learnable weight matrices, $\cup$ indicates the concatenation operation, and $\oplus$ represents the addition of channels.

Next, global average pooling is employed to extract the spatial information S_1 and S_2 from different channels. The SEWeight module is employed to capture channel attention weights, resulting in multi-scale attention weight vectors ω_i:

$$\omega_i = SEWeight(S_1 \oplus S_2) \tag{7}$$

These ω_i are adjusted using the Softmax function to derive the multi-scale channel recalibration weights att_i:

$$att_i = Softmax(\omega_i) = \frac{\exp(\omega_i)}{\sum_{i=0}^{S-1} \exp(\omega_i)} \tag{8}$$

Finally, the att_i are multiplied with the corresponding channels of Y' element-by-element to create the refined feature map Y as the output:

$$Y = Y' \bigotimes att_i \; i = 1, 2, 3, \cdots n-1 \tag{9}$$

Within the formula, $\bigotimes$ signifies channel-wise multiplication.

4. Construction of the Adaptive Denoising Residual Network Model

4.1. Optimized Residual Module

To mitigate noise interference in real industrial settings and improve the ability to extract key features from fault signals, this study optimizes the traditional residual module. The optimized residual building block (ORBB) is illustrated in Figure 5. The main enhancements include the following aspects:

i. Integrating SADNet into the residual module. For highly noisy signals, the spatial-adaptive denoising network employs a multi-scale encoder−decoder architecture to sample and weigh features at various scales. It estimates offsets, removing noise and reconstructing textures progressively from coarse to fine.

ii. Replacing the standard convolutional layers in traditional residual blocks with IPSA modules. For denoised signals, the improved pyramid split attention module captures channel attention vectors, multi-scale spatial information, and key cross-dimensional features within the channel attention vectors. This approach not only minimizes redundant computations but also boosts the learning of representative features.

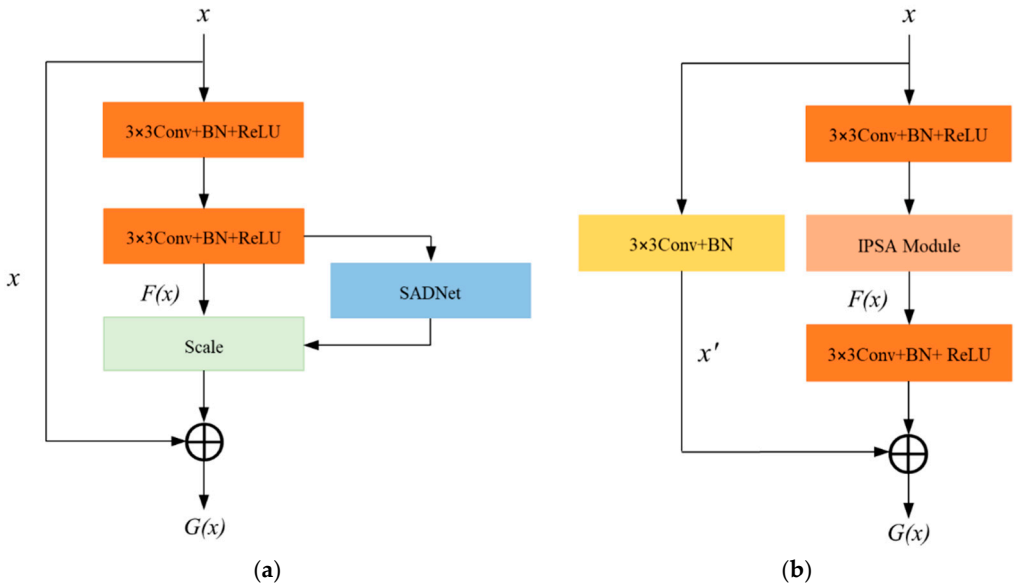


Figure 5. Optimized residual building block: (**a**) ORBB1; (**b**) ORBB2.

4.2. Adaptive Denoising Residual Network (AD-ResNet) Model

The AD-ResNet-based rolling bearing fault diagnosis model comprises convolutional layers, pooling layers, Block1, Block2, Block3, and fully connected layers, as depicted in Figure 6. To transform one-dimensional vibration signals from the time domain to the time-frequency domain, continuous wavelet transform is utilized, making the correlation information between fault signals more evident.

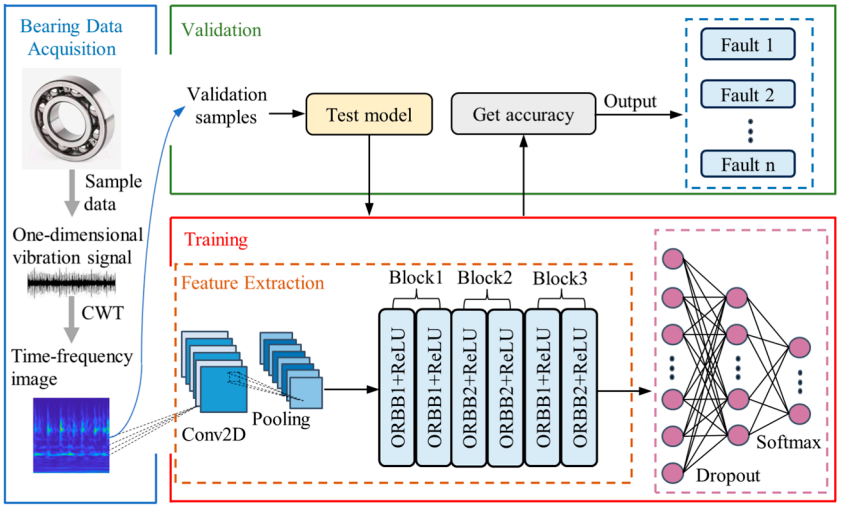


Figure 6. AD-ResNet model.

In the training phase, transformed time-frequency images are fed into the model proposed in this paper. Initially, we apply convolution along with max-pooling operations to capture superficial edge characteristics of the time-frequency map. Subsequently, deeper features are extracted using an arrangement of enhanced residual modules (Block1, Block2, and Block3) to increase the network depth. Integrating the SADNet structure within the residual module aids in eliminating image noise, reconstructing texture details, and bolstering the capacity to identify deep essential features. Next, Dropout is utilized prior to the fully connected layer to probabilistically disable certain neurons, promoting the acquisition of more robust information and reducing the risk of overfitting. Different fault types are classified using a Softmax classifier. After numerous iterations, the model

undergoes training and reaches convergence. In the validation phase, the trained model is utilized for diagnostic assessment on the test set to appraise its recognition effectiveness and generalization strength.

5. Experimental Validation

To assess the model's noise robustness, universality, and generalization capability of the proposed model, this paper conducts experimental analysis using the bearing datasets from Case Western Reserve University (CWRU) [39] and Huazhong University of Science and Technology (HUST) [40]. Performance metrics including precision, recall, F1-Score, and accuracy were utilized to assess the model's noise resistance and generalization capabilities. These performance metric formulas were defined as follows:

$$Precision = \frac{TP}{TP + FP} \tag{10}$$

$$Recall = \frac{TP}{TP + FN} \tag{11}$$

$$Accuracy = \frac{TP + TN}{TP + TN + FP + FN} \tag{12}$$

$$F1 - score = \frac{2 \times Precision \times Recall}{Precision + Recall} = \frac{2TP}{2TP + FP + FN} \tag{13}$$

In these formulas, TP represents the count of positive samples accurately predicted as positive, FN denotes the count of positive samples wrongly predicted as negative, FP indicates the count of negative samples incorrectly predicted as positive, and TN refers to the count of negative samples accurately predicted as negative.

5.1. Model Configuration and Parameter Settings

The experimental validation parameters laid out in this paper included the following: hardware configuration using an RTX A5000 (24 GB) GPU as the training method. The experimental environment comprised Python 3.8, Pytorch 1.10.0, and Cuda 11.1. For all experiments carried out in this study, the Adam optimizer was utilized for weight updating, with a learning rate of 0.001, a batch size of 32, a dropout rate of 0.5, and ReLU serving as the activation function. Detailed model parameter configurations are provided in Table 1.

Table 1. Model parameter settings.

Structure Name	Structure Parameters	Output Dimensions
Conv	$(3 \times 3 \times 32)$	64×64
Pooling-1	(2×2)	32×32
Block1	$\begin{pmatrix} 3 \times 3 \times 32 \\ 3 \times 3 \times 32 \end{pmatrix}$	32×32
Block2	$\begin{pmatrix} 1 \times 1 \times 16 \\ 1 \times 1 \times 128 \end{pmatrix}$	16×16
Block3	$\begin{pmatrix} 3 \times 3 \times 64 \\ 1 \times 1 \times 64 \\ 1 \times 1 \times 256 \end{pmatrix}$	4×4
Pooling-2	(2×2)	2×2
FC	—	256
Softmax	—	10

5.2. Analysis of the CWRU Bearing Dataset Experiments

5.2.1. Description of the Dataset

The dataset from CWRU, which was utilized for examining vibration signals, was gathered from the drive-end of the motor housing. The bearing under test was an SKF6205 motor bearing, operating at a speed of 1797 r/min. Figure 7 illustrates the experimental setup. The motor operated under load conditions of 0 HP, 1 HP, 2 HP, and 3 HP, with a sampling frequency of 12 kHz. This dataset encompassed both normal conditions and three fault categories: inner race fault (IR), outer race fault (OR), and ball fault (B). For each fault type, damage sizes of 0.007 inches, 0.014 inches, and 0.021 inches were included [39], resulting in a total of nine fault conditions plus one normal condition, summing up to ten categories. The data for each category were sampled using an overlapping window of length 1024 and then partitioned into training, validation, and testing sets in a ratio of 6:2:2. The experimental data statistics are provided in Table 2.

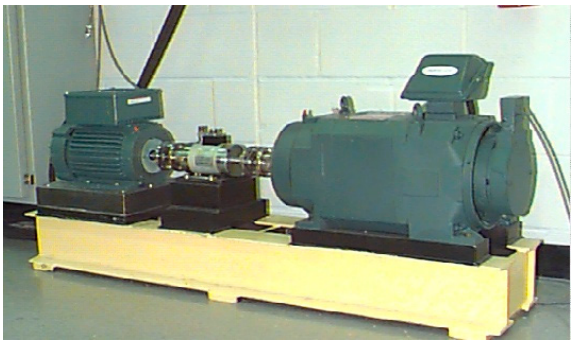


Figure 7. CWRU bearing test rig [39].

Table 2. Data description.

Fault Size	Type	Sample Quantity	Label
0	Normal	500	0
0.007	IR	500	1
	OR	500	2
	B	500	3
0.014	IR	500	4
	OR	500	5
	B	500	6
0.021	IR	500	7
	OR	500	8
	B	500	9

5.2.2. Noise Resistance Analysis of the Proposed Model

In real industrial settings, sensors that collect bearing vibration signals often face various noise interferences. In this section, to simulate different levels of environmental noise, 0 HP bearing data were used as experimental samples, and Gaussian white noise with SNRs of −4 dB, −2 dB, 0 dB, 2 dB, and 4 dB was added to the test set. To evaluate the noise resistance of the proposed model (AD-ResNet), its performance was contrasted with several commonly used deep learning models: VGG16, ResNet18, WDCNN [12], SADNet [36], and EPSANet [37]. The average outcomes from five experimental runs were considered for the final evaluation, as shown in Figure 8.

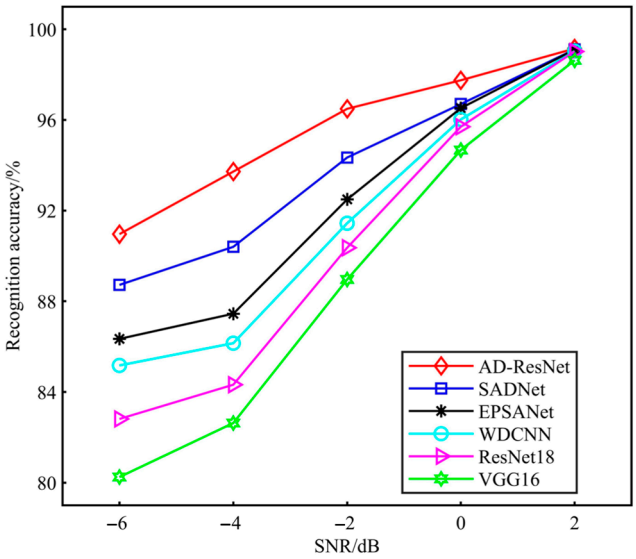
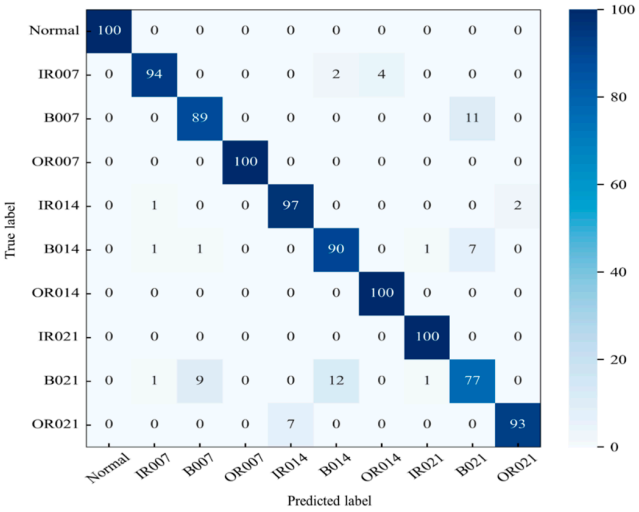


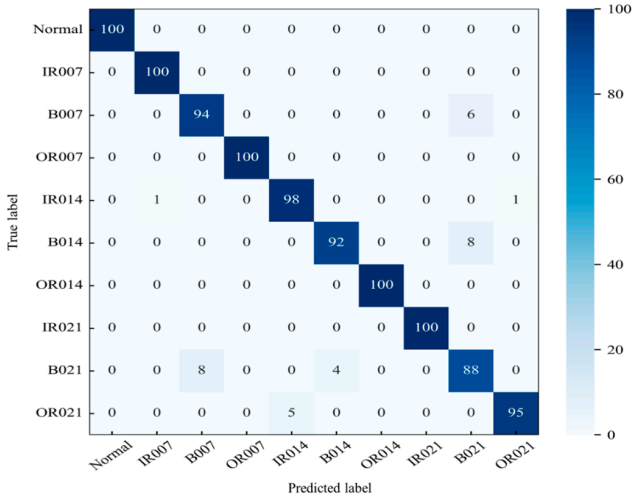
Figure 8. Accuracy of six models' recognition performance under varying SNR conditions.

According to Figure 8, AD-ResNet achieves the highest accuracy under SNR conditions ranging from −6 dB to 2 dB. Specifically, under the −6 dB strong noise condition, AD-ResNet attains an average accuracy of 90.96%. By contrast, the accuracies for the VGG16, ResNet18, WDCNN, IPSANet, and SADNet models are 80.25%, 82.81%, 85.17%, 86.34%, and 88.72%, respectively. Thus, the proposed model's accuracy surpasses these five models by 10.71%, 8.15%, 5.79%, 4.62%, and 2.24%, respectively. With a −2 dB SNR, AD-ResNet achieves an average accuracy of 96.49%, outperforming the SADNet model by 2.15% and 7.53% higher than the VGG16 model. Table 3 displays the comparative outcomes of different performance metrics under an SNR of −4 dB. These results suggest that AD-ResNet considerably outperforms the other five models in every metric. Specifically, AD-ResNet exhibits recall improvements of 3.47% and 6.31% compared to SADNet and EPSANet, respectively, highlighting its improved proficiency in recognizing positive instances and more effectively identifying fault categories. Regarding precision, the model demonstrates enhancements of 2.85% and 6.09%, showing that a greater proportion of actual faults are among the identified positive fault samples, thus decreasing false positive occurrences. The F1-score advances by 3.16% and 6.2%, indicating the model's superior overall effectiveness in maintaining a balance between precision and recall, thereby emphasizing AD-ResNet's enhanced classification abilities. Moreover, AD-ResNet's accuracy rises by 9.4% and 7.57% when compared to ResNet18 and WDCNN, respectively. The table reveals that, because of the relatively balanced fault category distribution within the dataset, accuracy provides a more comprehensive view of the model's overall effectiveness. Therefore, accuracy is chosen as the primary metric for performance evaluation in subsequent experiments. To further illustrate the effectiveness of AD-ResNet, confusion matrices were employed to visually represent the recognition of rolling bearing conditions in the test set. Figure 9 displays the confusion matrices for the ResNet, WDCNN, SADNet, and proposed models under the −6 dB SNR condition. The horizontal axis indicates predicted labels, while the vertical axis shows target labels. A predicted label equal to the actual label with a value of 100 signifies perfect classification. As depicted in the confusion matrix of AD-ResNet in Figure 9c, the lowest diagnostic accuracy among the 10 fault types is 91%, corresponding to the 0.014-inch OR, where 7% is misclassified as the 0.021-inch OR. The confusion matrix for the ResNet18 model, as depicted in Figure 9a, indicates that the accuracies for all three sizes of outer ring faults do not exceed 90%, with the 0.021-inch outer ring fault having an accuracy of only 77%. In Figure 9b, the SADNet model's confusion matrix shows that 6%

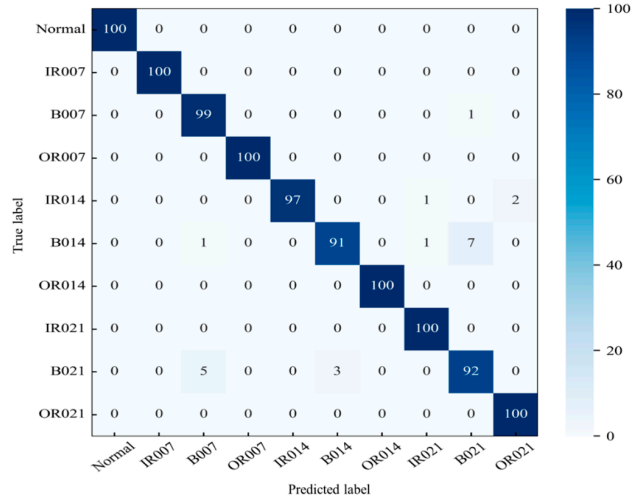
and 8% of the 0.007-inch and 0.014-inch OR, respectively, are misclassified as the 0.021-inch OR. These results indicate that, under strong noise conditions, other models show lower accuracies in identifying same-type faults of different sizes, while the proposed model is less impacted by noise and maintains high recognition accuracy and stability.



(**a**)



(**b**)



(**c**)

Figure 9. Confusion matrix plot of three different models under high noise: (**a**) ResNet18; (**b**) SADNet; (**c**) model in this paper.

Table 3. Comparison of various performance metrics at a signal-to-noise ratio of −4 dB.

Model	Performance Metrics			
	Precision (%)	**Recall (%)**	**Accuracy (%)**	**F1-Score (%)**
ResNet18	86.71	85.19	84.32	85.94
WDCNN	87.00	86.15	86.15	86.57
EPSANet	88.04	87.53	87.45	87.78
SADNet	91.28	90.37	90.40	90.82
AD-ResNet	94.13	93.84	93.72	93.98

5.2.3. Generalization Performance Analysis Under Different Load Conditions

Bearings in industrial environments usually operate under a variety of load conditions; hence, strong generalization capabilities are essential for fault diagnosis methods. To evaluate the generalization capability of AD-ResNet, it was compared with WDCNN [12], ResNet18, SADNet [36], and EPSANet [37] in experiments involving varying load conditions. The final outcomes were derived from the average of five repeated experiments. The datasets with constant load were used as the training set, while datasets with different loads were used as the test set. For instance, "1→2" denotes training with data under a 1 hp load and testing with data under a 2 hp load. Figure 3 illustrates the experimental results.

According to Figure 10, WDCNN and ResNet18 show lower diagnostic accuracy under different load conditions, with average recognition accuracies of 91.98% and 92.61%, respectively. Specifically, WDCNN achieved a recognition accuracy of 98.71% under "1→2" but only 85.50% under "2→1", indicating that early fault diagnosis models have diminished generalization capabilities under complex conditions. Conversely, the average accuracy of AD-ResNet is 96.99%, showing improvements of 4.38%, 5.01%, 1.59%, and 1.87% over ResNet18, WDCNN, EPSANet, and SADNet, respectively. This demonstrates that the proposed model possesses improved generalization capabilities, making it appropriate for diagnosing bearing faults under varying load conditions. Figure 11 presents the t-SNE visualization of the Softmax layer distributions for WDCNN, EPSANet, and the proposed model under the "2→1" condition. As seen in Figure 11, aside from minor confusion in individual faults, the proposed model demonstrates excellent clustering effects for all other faults, signifying better feature extraction capability and generalization compared to the other models.

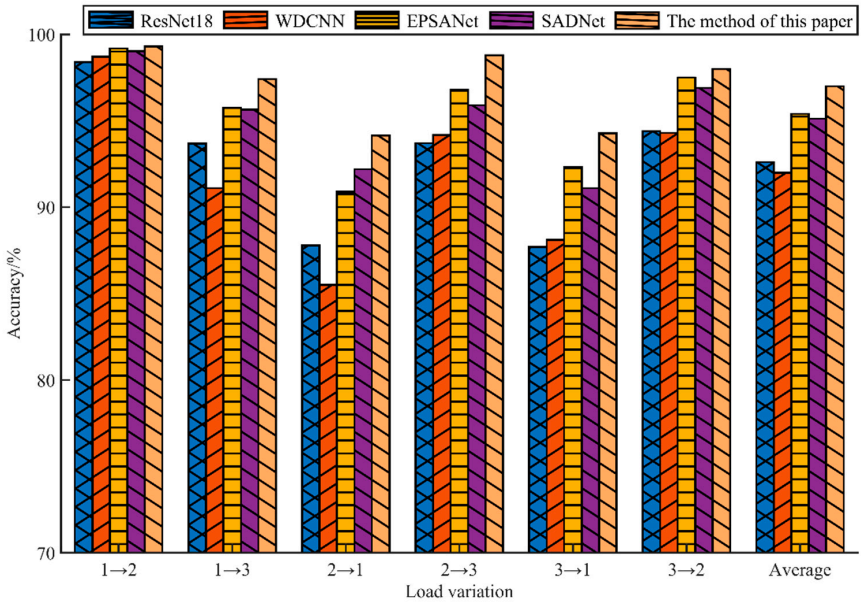


Figure 10. Accuracy of fault recognition under variable load.

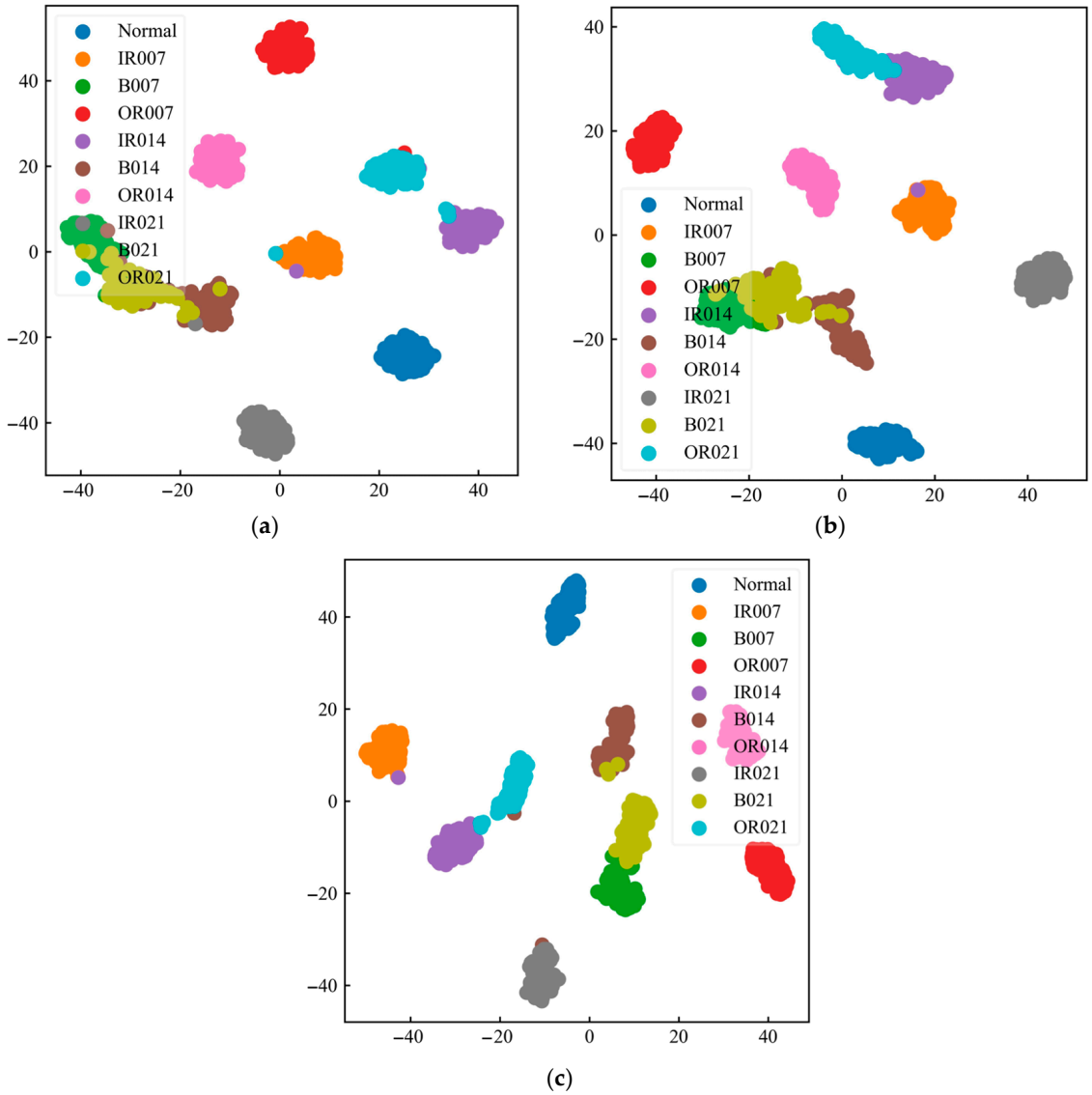


Figure 11. t-SNE visualization distribution of three different models: (**a**) WDCNN; (**b**) EPSANet; (**c**) model in this paper.

5.3. Experimental Analysis on the HUST Bearing Dataset

5.3.1. Description of the Dataset

Signal samples from the fault test rig were gathered in the HUST dataset, utilizing a sampling frequency of 25.6 kHz and rotational speeds of 3900 rpm, 4200 rpm, 4500 rpm, and 4800 rpm [40]. Besides the normal state (Normal), this dataset contains four distinct types of bearing faults: ball fault (B), outer ring fault (OR), inner ring fault (IR), and compound fault (C) [40]. Each fault category was further divided into two severity levels: moderate (M) and severe (S). Consequently, the dataset comprised eight fault conditions along with one normal condition, totaling nine categories. Data for each category were sampled using an overlapping window of length 1024. The dataset division was the same as CWRU. Table 4 illustrates the experimental data statistics.

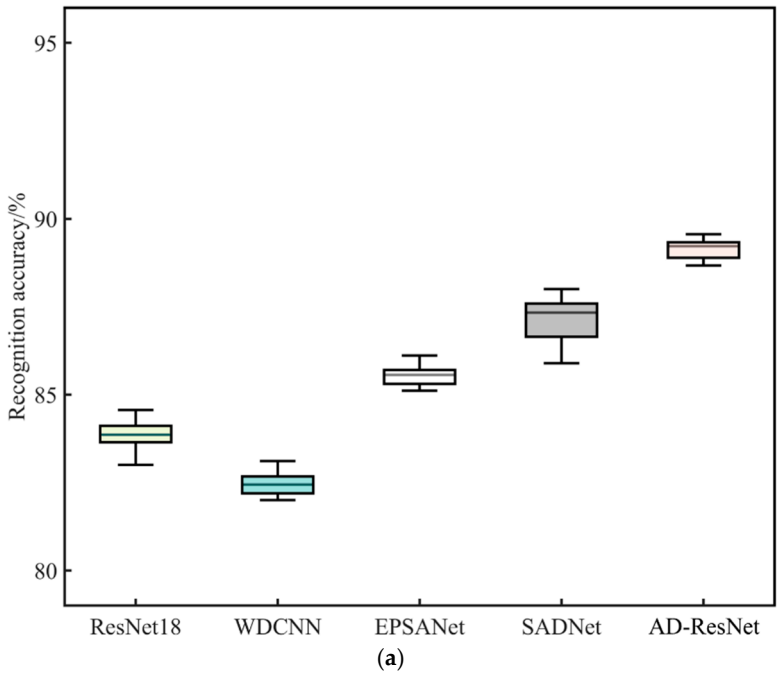
Table 4. Data description.

Fault Size	Type	Sample Quantity	Label
Normal	None	500	0
IR	M	500	1
OR	M	500	2
B	M	500	3
C	M	500	4
IR	S	500	5
OR	S	500	6
B	S	500	7
C	S	500	8

5.3.2. Boxplot Analysis of the Noise Resistance Performance of the Proposed Model

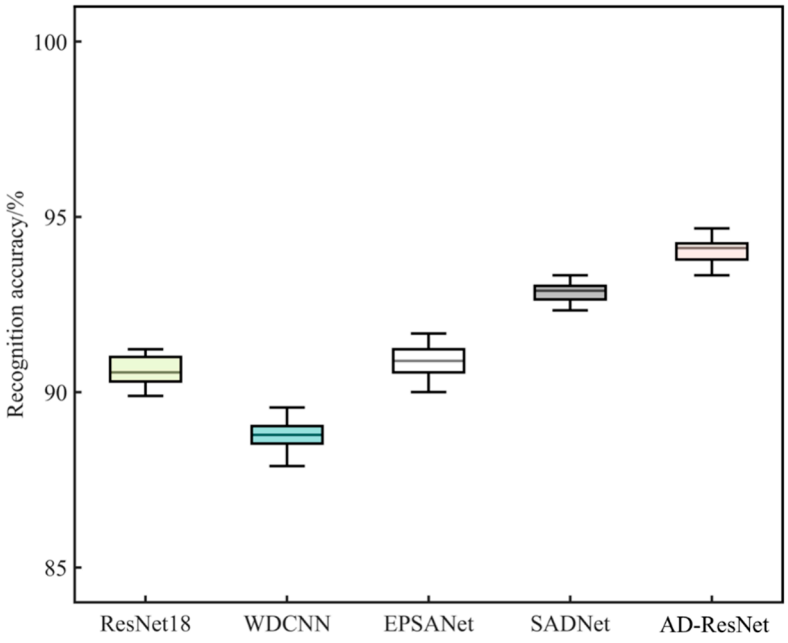
To further assess the noise resistance capability of the proposed AD-ResNet, boxplots were used to compare its performance with WDCNN [12], ResNet18, SADNet [36], and EPSANet [37]. Gaussian white noise with SNRs of −4 dB and −2 dB was introduced into samples at a rotational speed of 3900 r/min for experimental purposes. The findings from these tests are presented in Figure 12.

As demonstrated in Figure 12, AD-ResNet outperforms the other models by achieving the highest fault recognition rate and better stability under high noise conditions. This superior performance is attributed to the integration of the SADNet structure. Figure 12a indicates that, in comparison with the other four models, AD-ResNet showcases the highest average value and the smallest fluctuations, owing to the robust feature extraction capability provided by the IPSA module. These results demonstrate that the proposed model markedly enhances fault recognition rates under noisy conditions and exhibits strong robustness.



(**a**)

Figure 12. *Cont.*



(**b**)

Figure 12. Boxplot of recognition accuracy of different models: (**a**) SNR of −4 dB; (**b**) SNR of −2 dB.

5.3.3. Generalization Performance Analysis Under Different Rotational Speeds

To further evaluate the generalization performance of AD-ResNet in noisy environments, comparative experiments were carried out using VGG16, ResNet18, WDCNN [12], SADNet [36], and EPSANet [37] models under different rotational speeds. The final outcomes were derived from the average of five repeated trials. Samples were divided into datasets A, B, and C based on rotational speeds of 3900, 4200, and 4500 r/min, respectively. Gaussian white noise with an SNR of −2 dB was then added to each dataset. Constant load datasets served as training sets, while varying load datasets were used for testing. For instance, "A→B" means training on dataset A and testing on dataset B. Table 5 illustrates the experimental results.

Table 5. Recognition accuracy of six different models under variable speed conditions.

Model	Operating Condition							Average Training Time/s
	A→B	A→C	B→A	B→C	C→A	C→B	AVG	
VGG16	72.11	66.83	69.89	72.39	70.17	79.11	71.75	216.81
ResNet18	82.67	74.43	78.50	75.41	83.22	86.28	80.09	346.81
WDCNN	79.06	68.22	78.31	73.78	78.50	84.06	76.99	266.38
EPSANet	84.22	79.60	80.72	80.61	87.39	88.83	83.56	353.25
SADNet	86.31	84.43	83.86	84.33	89.17	89.61	86.28	386.12
AD-ResNet	90.11	87.89	87.01	88.83	91.72	91.67	89.54	365.69

According to Table 5 under six different rotational speed conditions, AD-ResNet achieved an average recognition accuracy of 89.54%, outperforming all other models. Compared to ResNet18 and EPSANet, the model showed improvements of 9.28% and 5.81%, respectively. This indicates that integrating the SADNet structure into the residual network significantly enhances feature extraction capabilities under high noise conditions, improving adaptability to variable rotational speeds. Furthermore, the model's average recognition accuracy increased by 3.09% compared to the SADNet model and shortened the average training time by 20.43 s. This demonstrates that the IPSA module effectively extracts representative features from channel attention vectors. Overall, the proposed

model maintains strong fault recognition capability and generalization performance under varying speed conditions accompanied by strong noise.

6. Conclusions

This research targets the challenges introduced by complex operational conditions and pronounced noise in real-world industrial environments, which can easily result in the incorrect identification of fault features and limited generalization capability. In response, we have refined and enhanced the ResNet model, achieving the following outcomes:

(1) Embedding the SADNet network structure into the residual block enables the model to weigh and extract multi-scale information from spatially relevant features. This tackles the challenges of complex feature extraction and poor fault recognition accuracy due to noise, enhancing the model's resistance to it. The IPSA module, replacing the standard convolution layers in the residual block, allowing the model to emphasize target-related feature channels while reducing the influence of irrelevant ones, boosts the model's capacity to extract features from channel attention vectors.

(2) Fault diagnosis experiments were carried out using the CWRU and HUST bearing datasets. In noise resistance analysis experiments, the proposed model's fault recognition accuracy under noise conditions with SNRs ranging from -6 to 2 dB was higher than other methods, with an average recognition rate of 90.96% under -6 dB Gaussian white noise. In load variation analysis experiments, the average recognition rate was 96.99%. In rotational speed variation noise resistance analysis experiments, the proposed model maintained the highest overall average recognition rate compared to other methods, demonstrating good noise resistance and generalization capabilities.

(3) Through a series of comparative experiments, we thoroughly confirmed the outstanding performance of the AD-ResNet model in both ideal conditions and challenging environments with strong noise and complex variables like speed and load changes. This research holds practical significance for diagnosing rolling bearing faults and offers a viable solution for intelligent fault diagnosis.

We also acknowledge potential limitations and areas for enhancement in this work. Firstly, despite the model exhibiting marked advancements in noise resilience and similar fault feature extraction, its effectiveness in fault identification could be compromised under scenarios with increased data volumes and noise intensity. Secondly, to mitigate the heightened time cost associated with the RSAB module, future work should focus on incorporating lightweight feature extraction modules (such as inverted residual blocks [41] or wavelet convolution layers [42]) and refining training strategies to further exploit the AD-ResNet model's capabilities.

Author Contributions: Conceptualization, Y.C. and X.Z.; methodology, Y.C.; software, Y.C.; validation, Y.C.; formal analysis, Y.C. and X.Z.; investigation, Y.C.; resources, X.Z. and H.H.; data curation, Y.C.; writing—original draft preparation, Y.C.; writing—review and editing, Y.C. and X.Z.; visualization, Y.C.; supervision, X.Z. and H.H.; project administration, X.Z. and H.H.; funding acquisition, X.Z. and H.H. All authors have read and agreed to the published version of the manuscript.

Funding: This research was funded by the Fujian Province Natural Science Foundation (2024J01877); the Putian City Science and Technology Project (2023SZ3001PTXY09); the Fujian University Engineering Research Center of Disaster Prevention and Mitigation of Southeast Coastal Engineering Structures (JDGC03); the Graduate Research Innovation Project (yjs2024035).

Data Availability Statement: The data presented in this study are available on request from the corresponding author.

Conflicts of Interest: The authors declare no conflicts of interest.

References

1. Li, H.; Zhang, J.; Qin, X.; Sun, Y. Fault diagnosis method for rolling bearings based on short-time Fourier transform and convolution neural network. *J. Vib. Shock* **2018**, *37*, 124–131. [CrossRef]
2. Chen, T.; Wang, Z.; Yang, X.; Jiang, K. A deep capsule neural network with stochastic delta rule for bearing fault diagnosis on raw vibration signals. *Measurement* **2019**, *148*, 106857. [CrossRef]
3. Liu, R.; Yang, B.; Zio, E.; Chen, X. Artificial intelligence for fault diagnosis of rotating machinery: A review. *Mech. Syst. Signal Process.* **2018**, *108*, 33–47. [CrossRef]
4. Yu, L.; Qu, J.; Gao, F.; Tian, Y.; Wang, X. Feature extraction of weak vibration signal based on improved sparse coding. *Chin. J. Sci. Instrum.* **2017**, *38*, 711–717. [CrossRef]
5. Xiong, J.; Deng, C.; Huang, G. Extreme Learning Machine for Multilayer Perceptron. *IEEE Trans. Neural Netw. Learn. Syst.* **2016**, *27*, 809–821. [CrossRef]
6. Li, B.; Han, R.; He, Y.; Zhang, X.; Hou, J. Applications of the Improved Random Forest Algorithm in Fault Diagnosis of Motor Bearings. *Proc. CSEE* **2020**, *40*, 1310–1319. [CrossRef]
7. Wang, X.; Yan, W. Fault diagnosis of roller bearings based on the variational mode decomposition and SVM. *J. Vib. Shock* **2017**, *36*, 252–256. [CrossRef]
8. Rai, A.; Upadhyay, S. Bearing performance degradation assessment based on a combination of empirical mode decomposition and k-medoids clustering. *Mech. Syst. Signal Process.* **2017**, *93*, 16–29. [CrossRef]
9. Zhu, J.; Hu, T.; Jiang, B.; Yang, X. Intelligent bearing fault diagnosis using PCA–DBN framework. *Neural Comput. Applic.* **2020**, *32*, 10773–10781. [CrossRef]
10. Chen, X.; Yang, R.; Xue, Y.; Huang, M.; Ferrero, R.; Wang, Z. Deep transfer learning for bearing fault diagnosis: A systematic review since 2016. *IEEE Trans. Instrum. Meas.* **2023**, *72*, 1–21. [CrossRef]
11. Lei, Y.; Yang, B.; Jiang, X.; Jia, F.; Li, N.; Nandi, A.K. Applications of machine learning to machine fault diagnosis: A review and roadmap. *Mech. Syst. Signal Process.* **2020**, *138*, 106587. [CrossRef]
12. Zhang, W.; Peng, G.; Li, C.; Chen, Y.; Zhang, Z. A New Deep Learning Model for Fault Diagnosis with Good Anti-Noise and Domain Adaptation Ability on Raw Vibration Signals. *Sensors* **2017**, *17*, 425. [CrossRef] [PubMed]
13. Wang, H.; Xu, J.; Yan, R.; Gao, R. A new intelligent bearing fault diagnosis method using SDP representation and SE-CNN. *IEEE Trans. Instrum. Meas.* **2020**, *69*, 2377–2389. [CrossRef]
14. Xiong, J.; Deng, S.; Shi, D. Fault Diagnosis for Rolling Bearings Based on Improved Residual Network. *Bearing* **2020**, *11*, 50–55. [CrossRef]
15. Tian, K.; Dong, S.; Jiang, B.; Pei, X.; Tang, B.; Hu, X.; Zhao, X. A bearing fault diagnosis method based on an improved depth residual network. *J. Vib. Shock* **2021**, *40*, 247–254. [CrossRef]
16. Zhang, S.; Liu, Z.; Chen, Y.; Jin, Y.; Bai, G. Selective kernel convolution deep residual network based on channel-spatial attention mechanism and feature fusion for mechanical fault diagnosis. *ISA Trans.* **2023**, *123*, 369–383. [CrossRef] [PubMed]
17. Chu, C.; Ge, Y.; Qian, Q.; Hua, B.; Guo, J. A novel multi-scale convolution model based on multi-dilation rates and multi-attention mechanism for mechanical fault diagnosis. *Digit. Signal Process.* **2022**, *122*, 103355. [CrossRef]
18. Hou, Y.; Wang, J.; Chen, Z.; Ma, J.; Li, T. Diagnosisformer: An efficient rolling bearing fault diagnosis method based on improved Transformer. *Eng. Appl. Artif. Intell.* **2023**, *124*, 106507. [CrossRef]
19. Ji, M.; Zhao, G. DEViT: Deformable Convolution-Based Vision Transformer for Bearing Fault Diagnosis. *IEEE Trans. Instrum. Meas.* **2024**, *73*, 1–13. [CrossRef]
20. Zhang, W.; Li, X.; Ding, Q. Deep residual learning-based fault diagnosis method for rotating machinery. *ISA Trans.* **2019**, *95*, 295–305. [CrossRef]
21. Che, C.; Wang, H.; Ni, X.; Fu, Q. Intelligent fault diagnosis method of rolling bearing based on stacked denoising autoencoder and convolutional neural network. *Ind. Lubr. Tribol.* **2020**, *72*, 947–953. [CrossRef]
22. Han, H.; Wang, H.; Liu, Z.; Wang, J. Intelligent vibration signal denoising methodbasedonnon-localfully convolutional neuralnet-workforrollingbearings. *ISA Trans.* **2022**, *122*, 13–23. [CrossRef]
23. Zhang, T.; Liu, S.; Wei, Y.; Zhang, H. A novel feature adaptive extraction method based on deep le-arning for bearing fault diagnosis. *Measurement* **2021**, *185*, 110030. [CrossRef]
24. Lei, C.; Xia, B.; Xue, L.; Jiao, M.; Zhang, H. Optimized deep residual network and its application in fault diagnosis of rolling bearing under the strong noise condition. *J. Vib. Eng.* **2023**, *36*, 1754–1763. [CrossRef]
25. Fu, L.; Wang, S.; Chen, R.; Ma, Z.; Ma, J.; Yao, B. Intelligent Fault Diagnosis of Rolling Bearings Based on an Improved Empirical Wavelet Transform and ResNet Under Variable Conditions. *IEEE Sens. J.* **2023**, *23*, 29097–29108. [CrossRef]
26. Fu, Z.; Liu, Z.; Ping, S.; Li, W.; Liu, J. TRA-ACGAN: A motor bearing fault diagnosis model based on an auxiliary classifier generative adversarial network and transformer network. *ISA Trans.* **2024**, *149*, 381–393. [CrossRef] [PubMed]
27. Sun, W.; Qin, Z.; Deng, H.; Wang, J.; Zhang, Y.; Zhang, K. Vicinity Vision Transformer. *IEEE Trans. Pattern Anal. Mach. Intell.* **2023**, *45*, 12635–12649. [CrossRef]

28. Yao, T.; Li, Y.; Pan, Y.; Wang, Y.; Zhang, X.; Mei, T. Dual Vision Transformer. *IEEE Trans. Pattern Anal. Mach. Intell.* **2023**, *45*, 10870–10882. [CrossRef] [PubMed]
29. Zhang, Z.; Lei, Z.; Omura, M.; Hasegawa, H.; Gao, S. Dendritic Learning-Incorporated Vision Transformer for Image Recognition. *IEEE/CAA J. Autom. Sin.* **2024**, *11*, 539–541. [CrossRef]
30. Li, S.; Zhao, X. A lightweight multi-feature fusion vision transformer bearing fault diagnosis method with strong local sensing ability in complex environments. *Meas. Sci. Technol.* **2024**, *35*, 065104. [CrossRef]
31. Xu, Z.; Tang, X.; Wang, Z. A Multi-Information Fusion ViT Model and Its Application to the Fault Diagnosis of Bearing with Small Data Samples. *Machines* **2023**, *11*, 277. [CrossRef]
32. Zhang, L.; Gu, S.; Luo, H.; Ding, L.; Guo, Y. Residual Shrinkage ViT with Discriminative Rebalancing Strategy for Small and Imbalanced Fault Diagnosis. *Sensors* **2024**, *24*, 890. [CrossRef] [PubMed]
33. Du, J.; Li, X.; Gao, Y.; Gao, L. Integrated Gradient-Based Continuous Wavelet Transform for Bearing Fault Diagnosis. *Sensors* **2022**, *22*, 8760. [CrossRef]
34. He, K.; Zhang, X.; Ren, S.; Su, J. Deep Residual Learning for Image Recognition. In Proceedings of the 2016 IEEE Conference on Computer Vision and Pattern Recognition (CVPR), Las Vegas, NV, USA, 27–30 June 2016; pp. 770–778. [CrossRef]
35. Zhang, K.; Tang, B.; Deng, L.; Liu, X. A hybrid attention improved ResNet based fault diagnosis method of wind turbines gearbox. *Measurement* **2021**, *179*, 109491. [CrossRef]
36. Chang, M.; Li, Q.; Feng, H.; Xu, Z. Spatial-Adaptive Network for Single Image Denoising. *arXiv* **2020**, arXiv:2001.10291.
37. Zhang, H.; Zu, K.; Lu, J.; Zou, Y.; Meng, D. EPSANet: An Efficient Pyramid Split Attention Block on Convolutional Neural Network. *arXiv* **2021**, arXiv:2105.14447. [CrossRef]
38. Li, J.; Wen, Y.; He, L. SCConv: Spatial and Channel Reconstruction Convolution for Feature Redundancy. In Proceedings of the 2023 IEEE/CVF Conference on Computer Vision and Pattern Recognition (CVPR), Vancouver, BC, Canada, 17–24 June 2023; pp. 6153–6162. [CrossRef]
39. Smith, W.; Randall, R. Rolling element bearing diagnostics using the Case Western Reserve University data: A benchmark study. *Mech. Syst. Signal Process.* **2015**, *64*, 100–131. [CrossRef]
40. Zhao, C.; Zio, E.; Shen, W. Domain Generalization for Cross-Domain Fault Diagnosis: An application-oriented perspective and a benchmark study. *Reliab. Eng. Syst. Saf.* **2024**, *245*, 109964. [CrossRef]
41. Wang, R.; An, S.; Liu, W.; Li, L. Invertible Residual Blocks in Deep Learning Networks. *IEEE Trans. Neural Netw. Learn. Syst.* **2024**, *35*, 10167–10173. [CrossRef]
42. Han, G.; Chen, J.; Liu, L.; Wang, Z.; Zhang, F.; Abudurexiti, Y. An Interpretable CNN With Wavelet Group Policy Embedded for Intelligent Fault Diagnosis. *IEEE Trans. Instrum. Meas.* **2024**, *73*, 3510815. [CrossRef]

Disclaimer/Publisher's Note: The statements, opinions and data contained in all publications are solely those of the individual author(s) and contributor(s) and not of MDPI and/or the editor(s). MDPI and/or the editor(s) disclaim responsibility for any injury to people or property resulting from any ideas, methods, instructions or products referred to in the content.